Relation of Planar Hall and Planar Nernst effects in Thin Film Permalloy

D. Wesenberg, A. Hojem, R. K. Bennet, and B. L. Zink

Department of Physics and Astronomy,

University of Denver, Denver, CO 80208

(Dated: April 20, 2018)

Abstract

We present measurements of the Planar Nernst Effect (PNE) and the Planar Hall Effect (PHE) of nickel-iron (Ni-Fe) alloy thin films. We suspend the thin-film samples, measurement leads, and lithographically-defined heaters and thermometers on silicon-nitride membranes to greatly simplify control and measurement of thermal gradients essential to quantitative determination of magnetothermoelectric effects. Since these thermal isolation structures allow measurements of longitudinal thermopower, or the Seebeck coefficient, and four-wire electrical resistivity of the same thin film, we can quantitatively demonstrate the link between the longitudinal and transverse effects as a function of applied in-plane field and angle. Finite element thermal analysis of this essentially 2D structure allows more confident determination of the thermal gradient, which is reduced from the simplest assumptions due to the particular geometry of the membranes, which are more than 350 μm wide in order to maximize sensitivity to transverse thermoelectric effects. The resulting maximum values of the PNE and PHE coefficients for the Ni-Fe film with 80% Ni we study here are $\alpha_{\mathrm{PNE,max}} = 30$ nV/K and $\rho_{\mathrm{PHE,max}} = 2$ nΩ m, respectively. All signals are exclusively $\sin 2\theta$ symmetry with applied field, ruling out long-distance spin transport effects. We also consider a Mott-like relation between the PNE and PHE, and use both this and the standard Mott relation to determine the energy-derivative of the resistivity at the Fermi energy to be $\partial\rho/\partial E = 4.7 \times 10^{-7}$ Ω m/eV, which is very similar to values for films we previously measured using similar thermal platforms. Finally, using an estimated value for the lead contribution to the longitudinal thermopower, we show that the anisotropic magnetoresistance (AMR) ratio in this Ni-Fe film is two times larger than the magnetothermopower (MTEP) ratio, which is the first evidence of a deviation from strict adherence to the Mott relation between Seebeck coefficient and resistivity.

I. INTRODUCTION

Recent years have seen an intense effort to understand the interplay of thermal, electronic, and spin degrees of freedom in a wide range of nanoscale magnetic systems and devices. This new field of spincaloritronics continues to expand, driven by the promise of new potential routes to energy harvesting, information storage, and logic devices enabled by spin.[1–3] Though significant effort in the field now focuses on interactions of magnons and electrons at an interface between a magnetic insulator and a non-magnetic metal with strong spin-orbit coupling[4–7], interest in thermal generation of spin currents in purely metallic systems remains high[8–12]. Thermal gradients applied to metallic ferromagnets have by now been confirmed to generate spin accumulation and pure spin currents only when heating is applied on a very short length scale comparable to the spin diffusion length in the metallic ferromagnet[13–21], or in experimental configurations that rely on magnon spin transport over somewhat longer distances[22]. Experiments that probe thermal gradients on much longer length scales, especially when a thin film ferromagnet is heated on a bulk substrate, have proven to produce signals dominated by traditional magnetothermoelectric effects. Depending on the exact orientation of the thermal gradient on the film at the location of the voltage probes, these effects can involve the planar Nernst effect, the anomalous Nernst effect, or a combination[23–36] . Here the emphasis on the transverse effects (the Nernst effect being the thermal analog to the Hall effect) comes since the inverse spin Hall effect (ISHE)[37–40] is typically used to probe the presence of spin currents, such that the signal of interest should be a voltage transverse to the applied thermal gradient.

Since control of the direction of the thermal gradient is so critical in identifying the physical processes that produce transverse voltages when metallic FM thin films are heated, we have pioneered thermal isolation platforms where a 500 nm thick free-standing silicon-nitride membrane replaces the bulk substrate beneath the FM.[41,42] This effectively confines the thermal gradient to the plane of the thin film FM sample deposited on the membrane. Our first experiments designed to probe thermal generation of spin currents when an exclusively planar thermal gradient is applied to permalloy (Py, the nickel-iron alloy with 80% nickel content) and nickel thin films showed no sign of spin currents.[24] All magnetic-field dependent effects instead showed the symmetry of the planar Nernst effect (PNE),[43,44] as confirmed by other groups using similar suspended structures.[25,31,36] Further work also

showed the expected tight link between the magnetic field dependence of the standard Seebeck effect and the PNE,[45] though these studies left several open questions, including the physical origin of a scaling factor needed to explain the total signal size and the cause of a magnetic field-independent background transverse voltage.

Metallic ferromagnets show several important responses to currents and thermal gradients, which often share a common origin and are related by simple expressions. In the Seebeck effect, a longitudinal thermal gradient, $\vec{\nabla}T$ applied to a conducting sample along the x-direction excites phonons and electrons that transport energy through the film. When no steady-state current can flow through the sample, charge flows only until the electric field balances the heat flow through the film such that $E_x = -\alpha_{xx}\partial T/\partial x$. If the thermal gradient is uniform between the voltage measurement leads separated by ℓ, then $\Delta V = E_x\ell$, $\partial T/\partial x = \Delta T/\ell$, and the longitudinal thermopower or Seebeck coefficient is given by $\alpha = -\Delta V/\Delta T$ with ΔT the temperature difference across the sample. Furthermore, the Seebeck coefficient is related to the electrical resistivity of the sample, ρ, via the Mott equation:

$$\alpha = -\frac{\pi^2 k_B^2 T}{3e}\frac{1}{\rho}\left[\frac{\partial \rho}{\partial E}\right]_{E=E_F}. \quad (1)$$

The interaction between conduction electrons and sample magnetization adds additional electrical and thermoelectric effects in ferromagnetic metals. One example of this interaction is the anisotropic magnetoresistance (AMR), where spin-dependent spin-orbit scattering generates a change in $\rho(H)$ that depends on the angle of the magnetization with respect to current flow that is even in applied field H. Examination of Eq. 1 indicates that the field-dependence of ρ will be reflected in α.

In addition to longitudinal thermopower, ferromagnetic conductors exhibit transverse thermopowers, where a voltage develops in the direction perpendicular to the applied thermal gradient. The anomalous Nernst effect (ANE) and planar Nernst effect (PNE) are thermal analogs to the well-known anomalous Hall effect (AHE) and planar Hall effect (PHE) in FM metals. In these effects, spin-dependent scattering of electrons in the presence of the internal magnetic field of the ferromagnet adds transverse momentum, which leads to voltages in the $\hat{y}$-direction when either current or thermal gradient is applied in the $\hat{x}$ direction. In the ANE a magnetic field applied perpendicular to the plane of a sample and a $\vec{\nabla}T$ in the plane of a sample generates an electric field transverse to the applied $\vec{\nabla}T$. In contrast to the ANE,

the PNE depends on the angle between the in-plane sample magnetization and $\vec{\nabla}T$. The PNE coefficient is defined by[46]

$$\alpha_{\mathrm{PNE}}(\mathrm{H}) = \frac{1}{2}[\alpha(\mathrm{H}_{\parallel}) - \alpha(H_{\perp})]\sin 2\theta. \tag{2}$$

In this equation, $\alpha(\mathrm{H}_{\parallel})$ and $\alpha(H_{\perp})$ are longitudinal thermopower coefficients measured in external fields oriented parallel and perpendicular to the applied $\vec{\nabla}T$. θ is the angle between the film magnetization, $\vec{M}$, and $\vec{\nabla}T$. The resulting angular dependence of the PNE is proportional to $\sin 2\theta$. The transverse electric field generated is then $E_{\mathrm{y,PNE}} = \alpha_{\mathrm{PNE}}(H)\partial T/\partial x$ and again if the thermal gradient is uniform the transverse PNE voltage is

$$V_{\mathrm{T,PNE}} = \alpha_{\mathrm{PNE}(H)}\frac{\Delta T}{\ell}w, \tag{3}$$

where w is the width of the sample in the transverse direction. Thus the PNE is the thermal analog to the planar Hall effect, where transverse voltage is generated depending on the angle between applied current and in-plane magnetization with coefficient:

$$\rho_{PHE}(H) = \frac{1}{2}[\rho(H_{\parallel}) - \rho(H_{\perp})]\sin 2\theta. \tag{4}$$

Here, assuming uniform current density, the transverse electric field is $E_{\mathrm{y,PHE}} = \rho_{\mathrm{PHE}}(H)I/(t\cdot w)$, with the sample thickness t and width in the transverse direction w defining the cross-sectional area. The transverse PHE voltage is then

$$V_{\mathrm{T,PHE}} = \rho_{\mathrm{PHE}(H)}\frac{I}{\ell}w. \tag{5}$$

This shows that just as measurements of longitudinal $\rho(H)$ allow prediction of the planar Hall voltage, measurements of longitudinal $\alpha(H)$ allow prediction of the planar Nernst voltage. One powerful feature of our thermal isolation platforms is that all these quantities can be measured on the same sample. If the measured V_T do not match the expectations from Eqs. 3 and 5, this indicates that the simple assumptions regarding uniformity of current density and/or thermal gradient must be examined.

The ability to measure ρ_{PHE} and α_{PNE} on the same sample also allows a unique exploration of the existence of a Mott-like relation between the planar Hall and planar Nernst effects. A transverse Mott relation between the ANE and the AHE has been described theoretically and proven for dilute magnetic semiconductors[47,48], but the relation for planar transverse effects has not been explored or demonstrated to our knowledge. Our group and others

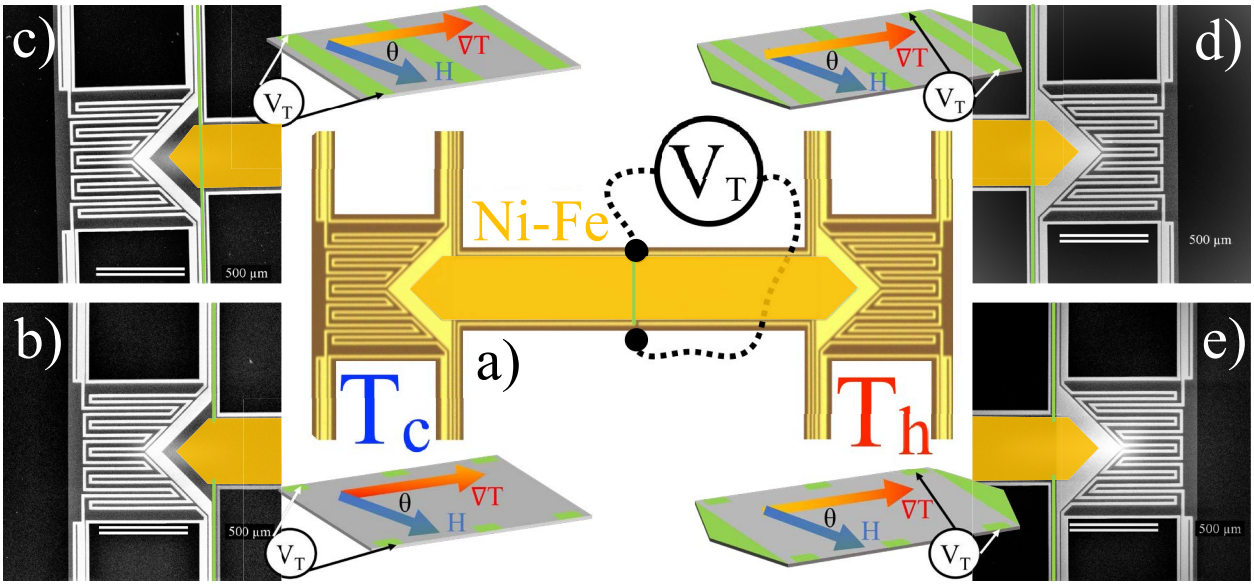

FIG. 1. Optical (center) and scanning electron microscope (black and white) images of thermal isolation platforms for PNE and PHE measurements. SEM images have accompanying schematics indicating location of electrical contact between Pt (green) and Ni-Fe film (highlighted in orange in micrographs) for V_{T} measurements. a) Optical image showing location of center voltage strip (green) contacts on Si-N bridge. The strip contact spans the entire width of the Ni-Fe film (orange). Lithographically patterned heaters and thermometers are seen on each island, indicated in yellow. b) "No shorts" Pt point contact variation on left island. The point contacts only make electrical contact several microns into each side of Ni-Fe. "No shorts" represents a reduced triangular lead to remove any electrical shorting to the film. c) "No shorts" Pt strip contact variation on left island. d) Pt strip contact variation on right island. e) Pt point contact variation on right island.

have previously shown that the Mott relation can be demonstrated in metallic FM samples by changing the values of ρ and α via applied magnetic fields at a fixed T[45,49,50]. These experiments have been interpreted by some as a demonstration that the energy derivative of ρ in Eq. 1 is independent of field, and can be used to determine a numerical value for this derivative. However, as we discuss further below, such demonstrations of the Mott relation as a function of applied field cannot rule out a field dependence of $\partial\rho/\partial E$ that has the same angular dependence as shown by the PNE and PHE themselves. Thus existing work cannot rule out an angular dependence of this derivative, leaving open the question of anisotropy of the scattering of electrons with applied field relative to the direction of applied gradients.

In this paper we present results from an optimized thermal isolation platform designed to more comprehensively probe thermal effects in thin film permalloy excited by well-controlled and quantified planar thermal gradients. These platforms employ wider samples than used in our earlier studies with both platinum strips and point contacts (as described in more detail below), in order to clarify the source of transverse voltages. We also produced platforms with no additional transverse electrical conduction path to examine closely any reduction in signal that these paths could produce. These platforms also allow voltage measurements on the same sample when either thermally biased or biased with an applied electrical current. This allows measurement of the planar Hall effect and the planar Nernst effect on exactly the same sample, and a close examination of the expected link between these various manifestations of spin-orbit scattering in metallic FM films. Since this comparison suggested disagreement when we used the simplest estimation of thermal gradient in the thermal isolation platform, we also performed 2d finite element modeling thermal analysis to calculate expected thermal gradients in the suspended structure as a function of position. Using the resulting thermal gradients gives excellent agreement between expected PNE and PHE signals and the corresponding Seebeck and anisotropic magnetoresistance values, comprehensively ruling out any signal corresponding to spin current generation in this mm-length scale experiment. Finally, we consider the form of a Mott relation between the planar Nernst coefficient and the planar Hall resistivity and compare this expectation to the Mott relation between longitudinal thermopower and electrical resistivity. The results show the same apparent field-independence of the scattering that was previously reported, though we add consideration of the field-dependence of the estimated absolute Seebeck effect that suggests a possibly anisotropy in the scattering with field direction.

II. EXPERIMENTAL DETAILS

We originally measured $\alpha(H)$, AMR and PNE in previous thermal isolation platforms of sizes much smaller than current platforms. Here we designed new platforms (Fig. 1) to further probe the potential long-range transverse spin Seebeck effect (tSSE) along with the PNE. We fabricated these using 500-nm-thick low-stress Si-N, with each platform micromachined from the same 100-mm Si wafer. We patterned 40-nm-thick Pt leads with a 10-nm-thick Cr adhesion layer via photolithography to serve as thermometers, heaters and

voltage leads. This extremely low thermal mass membrane yields effectively 2D heat flow and a unidirectional thermal gradient across the majority of bridge. We are able to measure four-wire electrical resistivity, longitudinal thermopower, and transverse voltages at three locations along Ni-Fe films. The sample studied here was grown on the Si-N structures before release from the Si substrate via e-beam evaporation from alloy source material under high vacuum (7×10^{-7} Torr) at 20 nm/s. The Si wafer was rotated during film deposition. The Si-N structures were subsequently released via deep-trench Si etching from the backside of the wafer.

As shown in Fig. 1, the updated thermal platforms consist of two 800 x 800 μm Si-N islands each connected to a supporting Si frame by 4 Si-N legs. The islands are connected with a bridge of length 2050-μm and width of 380-μm all suspended over a cavity. A 75-nm-thick NiFe film with width 353 μm was patterned on the bridge, which makes electrical contact with large Pt triangular leads for longitudinal thermopower and Pt voltage contacts for transverse voltage measurements. The platforms allow for "zero substrate" heating of our Ni-Fe thin films, which eliminates unintended thermal gradients and pushes our system to the 2D limit. Two varieties of voltage contacts are used for making transverse voltage measurements: strips (Fig. 1c) and d)) and point contacts (Fig. 1b) and e)) . These contacts are placed at either end of the film as well as the center. We also tested platforms with either point voltage contacts (Fig. 1b)) or Pt strips (Fig. 1c)) and no other metallic connections to the film, produced by removing the large triangular longitudinal thermopower measurement pads. These "no shorts" lead patterns eliminate any current shunting effects when measuring a transverse voltage on an island.

All measurements are taken using a cryostat under vacuum of 10^{-6} Torr or better to prevent convective heating. We mount the platforms to a radiation-shielded gold-plated copper mount to prevent radiative heating. Wire bonds are used to make connection with room-temperature electronics. Base temperatures of 276 K are used for all thermal measurements, so that raising the temperature of the platform island to 50 K above this base brings the average temperature of the sample itself near to room temperature, and 300 K for all electrical measurements. A small 20 μA current is used for resistance measurements to prevent film heating. We measure longitudinal thermopower by applying a series of heating powers to one island's heater. We then measure not only the voltage generated at either longitudinal or transverse contacts, but also the temperature of each island's separate sample thermome-

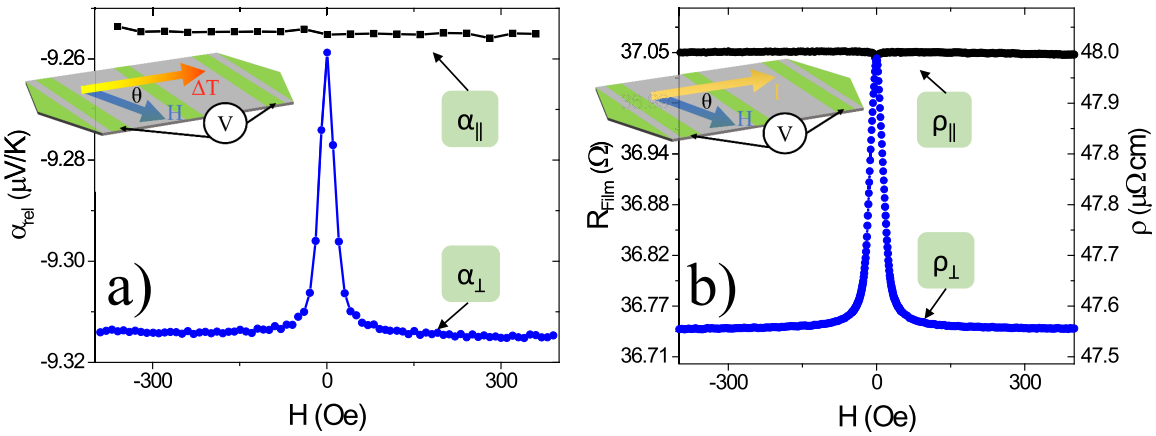

FIG. 2. Field dependence of α and ρ of Ni-Fe film. a) Longitudinal $\alpha_r el$ for both parallel and perpendicular field orientation. b) R and ρ for both parallel and perpendicular field orientation.

ter. We also monitor a similar micromachined resistive Pt thermometer on the supporting Si frame to ensure thermal stability during thermal measurements. Further details of thermopower measurements with the thermal isolation platforms are published elsewhere[45,51,52]. Transverse thermopower measurements are made by cycling a constant heating power on and off to remove any possible contribution from thermoelectric effects in cryostat wiring. The small mass of the membranes allows the islands to come to thermal equilibrium extremely rapidly ($\ll$ 1.5 s), which allows rapid collection of these heating cycles to improve signal-to-noise ratios. The platform allows easy reversal of the direction of thermal gradient by heating either island, but also allows measurements with near zero thermal gradient by heating both islands simultaneously to the same temperature. Further details on this quasi-ac technique for transverse voltage measurements were published previously[24]. Heat flow modeling was performed on the updated Si-N membranes using the Partial Differential Equation (PDE) toolbox from MATLAB[53]. The geometry of the membrane is imported directly from the photolithography layout files to define our model. The PDE toolbox uses a finite element analysis to define a 2D mesh geometry and formulate boundary conditions. Here we use a k_{2D} calculated by multiplying measured k values by thickness, t. Each layer has an additive contribution to total k_{2D}. Power was numerically applied uniformly to the geometry of the island heater, and chosen to achieve average island temperatures needed to model the experimental situations as required.

III. RESULTS

Fig. 2 displays longitudinal thermopower, $\alpha_{\rm rel}(H)$, and four-wire $R(H)$ at 300 K in perpendicular and parallel field orientations. The $R(H)$ measurements are typical of AMR in permalloy and show a film coercivity of $\sim$ 3 Oe in perpendicular and parallel configurations, about the same as seen on the narrower and thinner films previously measured[24,45]. As expected, at zero field and $\vec{M}$, both parallel and perpendicular orientations have similar values (the small difference in $\alpha_\parallel$ and $\alpha_\perp$ at $H = 0$ is most likely due to a small misalignment in the field angle for this measurement). $R(H)$ and $\alpha(H)$ exhibit similar, even field dependent patterns, indicating both are a result of spin-dependent scattering. $\Delta R/R$ for the various devices measured (not all are shown here) are in the $0.8 - 1\%$ range. We will use the quantities $\alpha_\parallel$, $\alpha_\perp$, $\rho_\parallel$, and $\rho_\perp$ in Eqs. 2 and 4 to determine the expected PNE and PHE coefficients.

Fig. 3 details transverse thermopower and PHE measurements made on Ni-Fe using a thermal isolation platform with point contacts (as shown in Fig. 1a) and e)). Panel a) shows transverse voltage V_T at the center of the platform bridge as a function of field for four different orientations of H with respect to ∇T. For example in the $\theta = 0^\circ$ orientation, ∇T is parallel to applied field. Also shown in each sub-panel are measurements for $\nabla T = 0$ (black symbols), $\nabla T = 14.9$ K/mm (red symbols) and $\nabla T = -14.9$ K/mm (blue symbols). As discussed in detail below, these values of thermal gradient are the result of 2d heat flow simulations and are significantly lower than the simple expectation based on the measured temperature difference between the islands. Note that heating both islands such that $\nabla T = 0$ gives a totally field-independent background voltage. Panel b) shows transverse voltage at the same center point contacts in response to applied charge current for $I = \pm 30$ μA and 15 μA. These show qualitatively similar patterns, though no background voltage appears in the PHE case since no significant temperature differences arise in the platform for these measurements.

Figs. 3c) and d) summarize the results of these experiments by plotting the saturated values of V_T as a function of the angle θ. In the case of thermal measurement for the , the $\nabla T = 0$ voltage was first subtracted though of course this does not alter the field dependence of the signal in any way. Here the $\sin 2\theta$ dependence of the PNE is clear, and the maximum value of these signals indicates a PNE component with voltage near 150 nV. As expected,

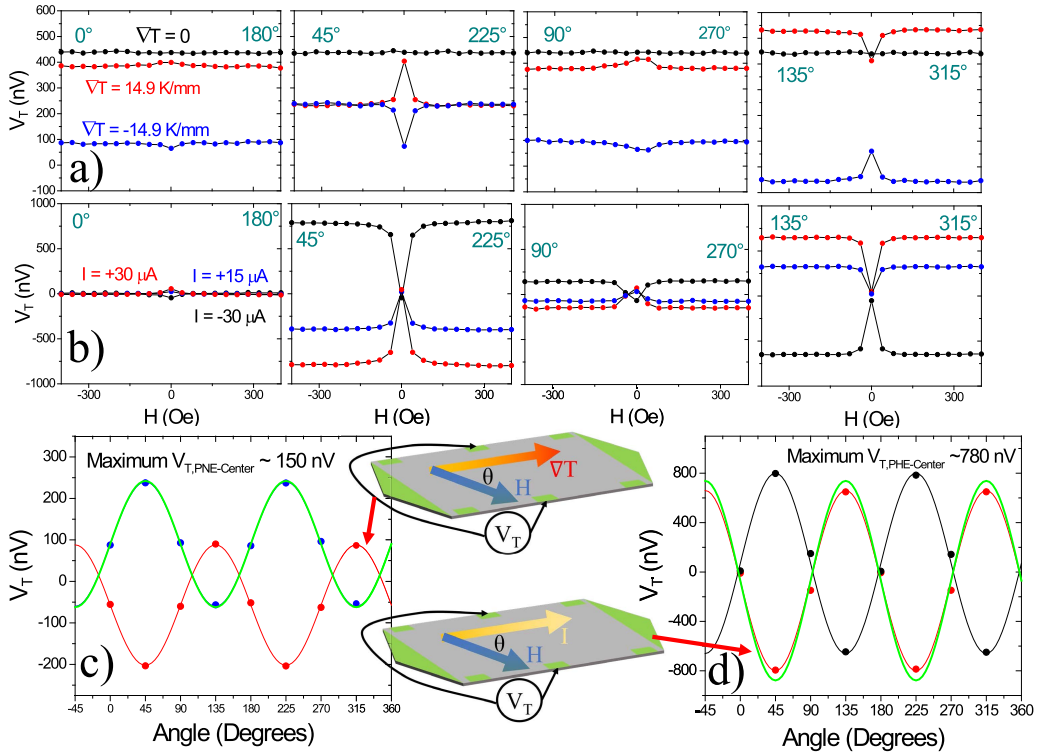

FIG. 3. Magnetic field dependence of V_T using point contacts at the center of the platform bridge as a function of angle for both applied T and I. a) V_T at center in response to applied thermal gradient, with four different field orientations. Black data points indicate zero thermal gradient (achieved by heating both membranes), red data points are $\nabla T = 14.9$ K/mm and blue are $\nabla T = -14.9$ K/mm. b) V_T at center in response to applied current, with four different field orientations. Black data points are for $I = -30$ μA, red $I = 30$ μA, and blue $I = 15$ μA c) Saturated V_T from a) vs. field orientation angle. Green line indicates predicted V_T calculated from Eq. 3. d) Saturated V_T from b) vs. field orientation angle. Green line indicates predicted V_T calculated from Eq. 5.

the purely electric measurement also shows the $\sin 2\theta$ dependence resulting from the PHE with $V_T = 780$ nV. In each plot the green line shows V_T predicted by Eq. 3 or 5, with the appropriate coefficient determined from the data in Fig. 2 using Eq. 2 or 4. The values of ∇T used here will be discussed in detail below.

Fig. 4 depicts the same series of experiments on the same Ni-Fe film, but with V_T measured at point contacts on the right end of the film near the triangular lead visible in Fig. 1e). Here for PNE experiments, the $\nabla T = 0$ background must only be removed from the orientation of ∇T that results in heating of the right island, since there is little temperature rise compared

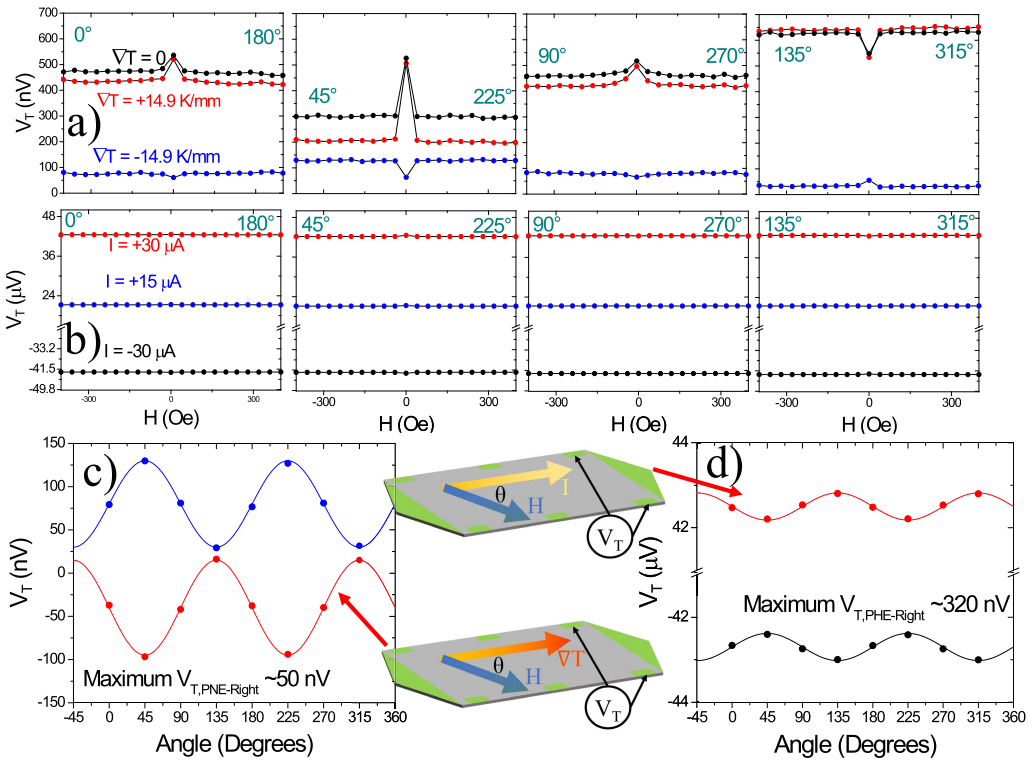

FIG. 4. Magnetic field dependence of V_T using point contacts on right side of the platform bridge as a function of angle for both applied T and I. a) V_T at right in response to applied thermal gradients, with four different field orientations. Black data points indicate zero thermal gradient (achieved by heating both membranes), red data points are $\nabla T = 14.9$ K/mm and blue are $\nabla T = -14.9$ K/mm. b) V_T at right in response to applied current, with four different field orientations. Black data points are for $I = -30$ μA, red $I = 30$ μA, and blue $I = 15$ μA. c) Saturated V_T from a) vs. field orientation angle. d) Saturated V_T from b) vs. field orientation angle.

to the base temperature on the non-heated island. The proximity of the measurement location to the triangle lead and to the island itself has a large effect on the signals measured, leading to an apparent field-dependence of the $\nabla T = 0$ background and adding large offset voltages to the PHE data. As shown in Figs. 4c) and d), the overall size of the PNE and PHE signals also drops, by a factor of three in the case of PNE and more than a factor of 2 for PHE, though the field dependence remains entirely $\sin 2\theta$.

As shown in Fig. 5, comparison of these results with platforms using Pt strips in both the standard and "no shorts" configurations clarifies the physics and puts an additional limit on any spin current generation in these mm-scale thermal experiments. Figs. 5a) and b) show

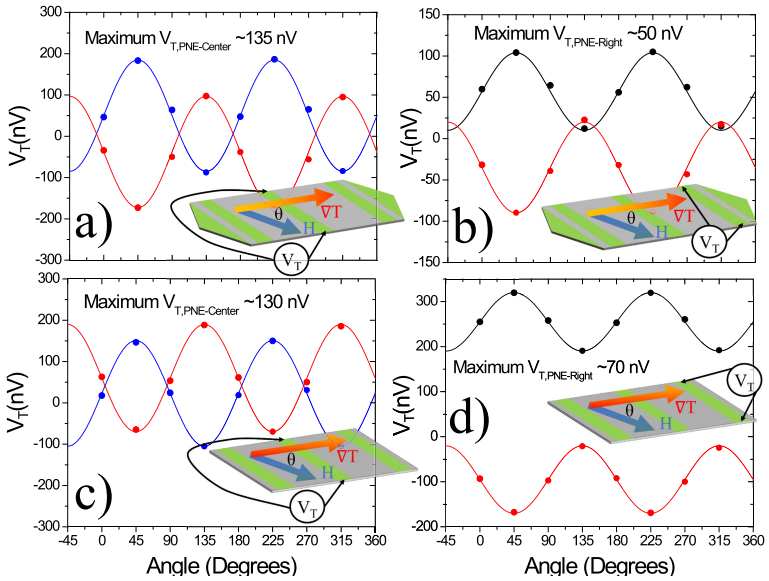

FIG. 5. V_T vs. angle comparing center and right side strip contacts as well as "no shorts" contacts. a) V_T vs. angle for center strip contacts. b) V_T vs. angle for right side strip contacts. c) V_T vs. angle for center strip contacts with "no shorts". d) V_T vs. angle for right strip contacts with "no shorts".

saturated V_T as a function of θ measured on Pt strips at the center of the bridge and right end, respectively. Both show exclusively $\sin 2\theta$ field dependence, with no sign of the $\cos\theta$ symmetry that would indicate presence of the transverse spin Seebeck effect (tSSE)[54] within the 10 nV accuracy of the measurements. Comparison of Fig. 5a) to Fig. 3c), where the same experiment was performed with point contacts, shows that the overwhelming effect of the Pt strip is to partially shunt the transverse voltage, such that the maximum measured PNE signal component is reduced from 150 nV to 135 nV. These shunting effects become greater near the triangular leads, though a significant reduction in the signal size to $\sim$ 70 nV occurs even with no transverse shorts. This indicates reduced and non-uniform thermal gradients, as the thermal simulations below bear out. Fig. 5c) shows that the center strip location is not meaningfully affected by removal of the triangular leads at the ends, as expected. The removal of the triangular leads also causes field-independent background voltages of opposite sign for the opposite orientations of ∇T as shown in Fig. 5d), a phenomenon also seen in the original thermal isolation platform experiments we used to demonstrate the PNE and search for the tSSE in metallic ferromagnets[24]. These results clearly show that such sign changes can easily be generated solely from non-uniform thermal gradients. None

of the saturated V_T measurements for Pt strips have ever shown larger voltages than the corresponding measurement with point contacts, which puts a firm limit on the presence of thermal spin current effects when truly in-plane thermal gradients are applied on mm-length scales in metallic FMs. Considering the elimination of uncertainty introduced by shunting effects and the increased length of the Pt detector strips used here, these results reduce the lower limit we previously placed on the tSSE coefficient[24] by more than a factor of three using the original definition of the $S_{\rm SSE}$ coefficient[55]. This upper limit (using the experimental parameters assumed in the original report) is $|S_{\rm SSE}| \leq 3.6 \times 10^{-12}$ V/K.

IV. DISCUSSION

According to Eqs. 2 and 4 and using the data from Fig. 2, we calculate the maximum value of the PNE coefficient that occurs when $\sin 2\theta = 1$, $\alpha_{PNE,max} = 30$ nV/K, and the maximum value of the PHE coefficient, $\rho_{PHE,max} = 2$ nΩ m. Using the geometry of the Ni-Fe film, the expected PHE transverse voltage signal from Eq. 5 is shown in Fig. 3d) as the green solid curve and has a maximum value of 800 nV. This is in excellent agreement with $V_{T,max} = 780$ nV measured for the PHE on the center point contacts, as is obvious in Fig. 3d). However, if we use the simple assumptions regarding thermal gradients that result in the expression in Eq. 3, we expect a thermal gradient near 23 K/mm and $V_{T,max} \sim 240$ nV. The actual measured values of this PNE voltage contribution even for the ideal case of the center point contacts are far lower (150 nV), indicating that the real thermal gradient at the center of the bridge of the thermal isolation platform is lower.

To explore this possibility in greater detail we performed 2D finite element analysis heat flow simulations in steady state using the actual geometry of our platforms imported directly from lithography layout files. As a first approximation, we use temperature independent thermal conductivities but take these values from our extensive experience using similar platforms to measure thermal conductivity of metallic thin films and the Si-N supporting structure[41,56]. Figure 6 reports results of these simulations, with panel a) showing the color-mapped solution of the thermal Laplace equation overlaid on the representation of the FEM mesh used in the calculation, and panel b) showing the resulting thermal gradient along the center of the sample bridge as a function of position x, for the three different heating conditions used in the PNE measurements. These simulations clearly show that

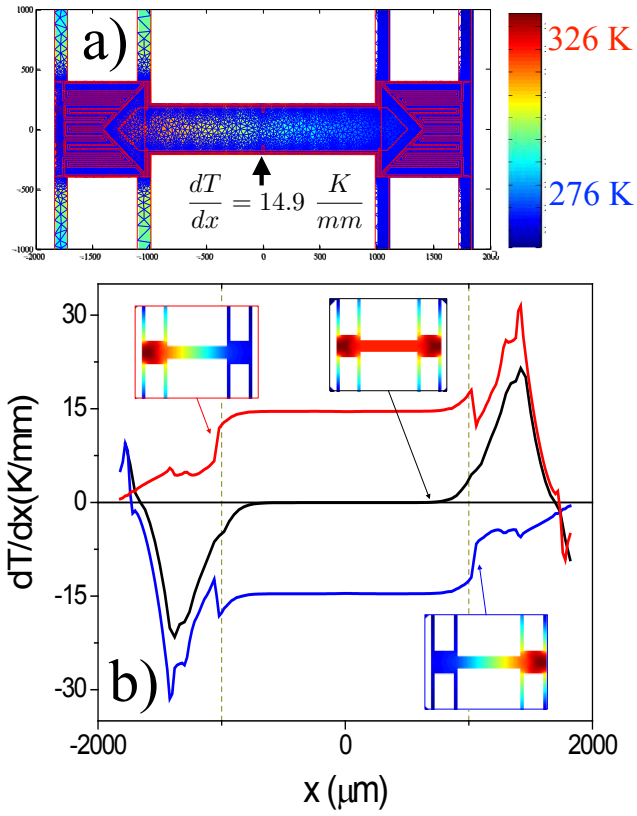

FIG. 6. 2D finite element analysis modeling of PNE structures using PDE toolbox from MATLAB. a) Color-mapped solution of the thermal Laplace equations overlaid on FEM mesh for left side heated. b) Temperature profiles down center length ($y = 0$) of membrane under various thermal load. Red line indicates left side heating with $\Delta T = 50$ K between left island and frame. Blue line indicates right side heating with $\Delta T = 50$ K between right island and frame. Black line indicates both left and right island heating with $\Delta T = 0$ K between islands and 50 K between islands and frame.

when the desired 50 K temperature difference between heated island and frame is achieved, the thermal gradient at the center of the bridge is very uniform for a large range of the structure, but indeed is much lower than the simple estimation. Using the simulated values of $\nabla T = \pm 14.9$ K/mm to predict the PNE V_T gives the green curve in Fig. 3c, which nearly exactly matches the measured V_T.

With this understanding of the thermal gradient and transverse shorting issues, we can also examine limits on the existence of the long-length scale thermal spin current generation, or tSSE, in metallic ferromagnets. The original reports of the tSSE suggested spin Seebeck

Sample	M_{Mott} $\left(\frac{\mathrm{V}}{\mathrm{K}}\Omega\mathrm{m}\right)$	$\partial\rho/\partial E$ $\left(\frac{\Omega\mathrm{m}}{\mathrm{eV}}\right)$	$\partial\rho/\partial E_{\mathrm{planar}}$ $\left(\frac{\Omega\mathrm{m}}{\mathrm{eV}}\right)$
Ni-Fe (75 nm)	-3.42×10^{-12}	4.7×10^{-7}	4.7×10^{-7}
Ni-Fe (20 nm)[45]	-2.6×10^{-12}	3.5×10^{-7}	-
Ni (20 nm)[45]	-2.8×10^{-12}	3.8×10^{-7}	-

TABLE I. Slope M_{Mott} and derivatives $\partial\rho/\partial E$ comparing three different membrane-supported FM metal films.

coefficients near 6×10^{-11} V/K for Ni-Fe. Using the geometry of the thermal isolation platforms discussed here, the resulting signal would be a $\cos\theta$ contribution with amplitude near 300 nV. Here we have conclusively shown no $\cos\theta$ signal within the ~ 10 nV error bar of our transverse voltage measurements. This puts a stringent limit on the existence of the tSSE, of $\approx 20\times$ lower than original reports.[55]

Finally, we can examine the question of a Mott-like relation between the PNE and PHE coefficients. Eq. 1 shows that at a fixed temperature, and if the energy derivative of ρ is independent of magnetic field, a plot of $\alpha(H)$ vs. $1/\rho(H)$ will be linear with a slope given by

$$M_{\mathrm{Mott}} = -\frac{\pi^2 k_B^2 T}{3e}\left[\frac{\partial\rho}{\partial E}\right]_{E=E_F}. \tag{6}$$

When examining the Mott relation involving the longitudinal Seebeck coefficient, one must measure multiple α and $1/\rho$ and determine this slope, since any measurement of longitudinal thermopower includes the contribution from the voltage lead itself. In other words, all measured longitudinal thermopower values are relative rather than absolute, such that $\alpha_{\mathrm{rel}} = \alpha_{\mathrm{film}} - \alpha_{\mathrm{lead}}$. Examining only the field dependence is one way to correct for this lead contribution, though this technique also throws away any portion of the sample thermopower that is field-independent. Since at fixed T the first fraction in Eq. 6 is entirely constant, determining this slope from the saturated values of α and ρ as shown in Fig. 2, allows calculation of the energy derivative of the electrical resistivity with respect to energy. This is a quantity that is difficult to measure directly, so these measurements have fundamental value for exploring the electron-energy dependence of the scattering events that contribute to ρ. The first two columns of Table I compare M_{Mott} and $\partial\rho/\partial E$ for the Ni-Fe thin film measured here, as well as Ni-Fe and Ni films previously measured by our group[45]. Despite

differences in thickness and growth technique (75 nm films were e-beam evaporated and 20 nm films were sputtered), the values for $\partial\rho/\partial E$ at $E = E_F$ are remarkably similar, varying by less than 25%.

As a first attempt at writing an expression that relates α_{PNE} and ρ_{PHE}, one might simply replace the corresponding longitudinal coefficients in Eq. 1, as is effectively the case for the ANE and PHE[47,48]. However, such an equation would suggest that decreasing ρ_{PHE} would increase α_{ANE}, which is not physically accurate. Instead we first assume the Mott relation holds separately for $\alpha_\perp$ and $\alpha_\parallel$, and use the definition of the PNE coefficient to determine the relationship:

$$\alpha_{\mathrm{PNE}} = -\frac{1}{2}\frac{\pi^2 k_{\mathrm{B}^2} T}{3e}\left(\frac{1}{\rho_\parallel}\left[\frac{\partial\rho_\parallel}{\partial E}\right]_{E=E_F} - \frac{1}{\rho_\perp}\left[\frac{\partial\rho_\perp}{\partial E}\right]_{E=E_F}\right)\sin 2\theta. \tag{7}$$

With the further assumption that

$$\left[\frac{\partial\rho_\parallel}{\partial E}\right]_{E=E_F} = \left[\frac{\partial\rho_\perp}{\partial E}\right]_{E=E_F} \equiv \left[\frac{\partial\rho}{\partial E}\right]_{E=E_F}, \tag{8}$$

and using Eq. 4, then

$$\alpha_{\mathrm{PNE}} = \frac{\pi^2 k_{\mathrm{B}^2} T}{3e}\frac{\rho_{\mathrm{PHE}}}{\rho_\parallel \rho_\perp}\left[\frac{\partial\rho}{\partial E}\right]_{E=E_F}. \tag{9}$$

As we have experimentally determined all coefficients in this equation apart from the energy derivative of ρ, we can determine $(\partial\rho/\partial E)_{\mathrm{planar}}$ directly as shown in Table I. The result exactly matches the quantity determined from the standard Mott relation, as expected based on the assumptions made in this calculation.

However, we note that any angular dependence of this derivative is likely to have the same functional dependence of the AMR and magnetothermopower, and the apparent agreement of the various values in Table I cannot reveal an anisotropy in the scattering because of the underlying assumption that the Mott relation holds for the separate field directions. However, we can examine this assumption more closely by comparing the AMR ratio and its thermal analog. By the traditional definition using the data shown in Fig. 2, the AMR ratio for our Ni-Fe sample is

$$\frac{\Delta\rho}{\rho_o} = \frac{\rho_\parallel - \rho_\perp}{\frac{1}{3}\rho_\parallel + \frac{2}{3}\rho_\perp} = 8.40 \times 10^{-3}. \tag{10}$$

The thermal analog is simple to write, but we clarify that this requires determination of the *absolute* Seebeck coefficient, which is challenging for thin film structures since thin films even

of nominally pure materials cannot be expected to have bulk values of the Seebeck coefficient. We have explored a number of techniques to approximate the lead contribution to longitudinal thermopower[57,58] and estimate a room-temperature contribution from the Pt leads used in these thermal isolation platforms to be $\alpha_{\text{lead}} = -5\ \mu\text{V/K}$. If we keep the definition of $\alpha_{\parallel}$ and $\alpha_{\perp}$ as relative thermopower used above, then the corrected magnetothermopower ratio is

$$\frac{\Delta\alpha}{\alpha_o} = \frac{\alpha_{\parallel} - \alpha_{\perp}}{\frac{1}{3}\alpha_{\parallel} + \frac{2}{3}\alpha_{\perp} + \alpha_{\text{lead}}} = 4.20 \times 10^{-3}, \tag{11}$$

which is a factor of two lower than for the AMR. Since typical error on relative thermopower measurements made with our thermal isolation platforms is on the order of several percent at most, the largest source of uncertainty in Eq. 11 is the estimated value of lead resistance. However, we point out that for the magnetothermopower ratio to equal the AMR ratio would require α_{lead} more than a factor of 3 larger in magnitude and of opposite sign. Such a large deviation in the estimated lead contribution is unlikely. This is the first indication of a break with the strict relationship between α and ρ prescribed by the Mott relation and may be the first evidence of a field-induced anisotropy between the thermally-driven and electric-field driven scattering of electrons in ferromagnetic metals.

In summary, we have used unique thermal isolation platforms to explore the relation between the planar Nernst effect and planar Hall effect in thin films of ferromagnetic metallic nickel-iron alloys. To confirm the uniformity of thermal and current gradients, we measured transverse voltages at various locations on the film, and explicitly tested the effect of transverse current shorting paths. The comparison between the current-driven planar Hall effect and the thermally-driven planar Nernst effect is extremely tight after the correct value of thermal gradient was determined for this structure using 2D finite element analysis. As all measured signals show field dependence of $\sin 2\theta$, these results put a stringent limit on the long-distance transverse spin Seebeck effect in ferromagnetic metals. Comparison of the AMR and magnetothermopower ratios, after estimation of the absolute Seebeck coefficients, is the first evidence of a possible deviation in field dependence of the thermal and current-based effects.

We thank S. J. Mason, and A. D. Avery for helpful discussions and assistance in the lab, X. Fan for sharing insight on transverse Mott relations, J. Nogan and the IL staff at CINT for guidance and training in fabrication techniques, D. Schmidt, J. Beall, G. Hilton, J. Nibarger

and the staff at the NIST Boulder Quantum Fabrication Facility for advice and assistance with deep trench Si etching, and gratefully acknowledge support from the NSF (DMR-1410247 and DMR-1709646). This work was performed, in part, at the Center for Integrated Nanotechnologies, an Office of Science User Facility operated for the U.S. Department of Energy (DOE) Office of Science by Los Alamos National Laboratory (Contract DE-AC52-06NA25396) and Sandia National Laboratories (Contract DE-AC04-94AL85000).

[1] S. R. Boona, R. C. Myers, and J. P. Heremans, Energy Environ. Sci. **7**, 885 (2014).

[2] G. E. W. Bauer, E. Saitoh, and B. J. van Wees, Nature Materials **11**, 391 (2012).

[3] G. E. W. Bauer, A. H. MacDonald, and S. Maekawa, Solid State Communications **150**, 459 (2010).

[4] F. Hellman, A. Hoffmann, Y. Tserkovnyak, G. S. D. Beach, E. E. Fullerton, C. Leighton, A. H. MacDonald, D. C. Ralph, D. A. Arena, H. A. Dürr, P. Fischer, J. Grollier, J. P. Heremans, T. Jungwirth, A. V. Kimel, B. Koopmans, I. N. Krivorotov, S. J. May, A. K. Petford-Long, J. M. Rondinelli, N. Samarth, I. K. Schuller, A. N. Slavin, M. D. Stiles, O. Tchernyshyov, A. Thiaville, and B. L. Zink, Rev. Mod. Phys. **89**, 025006 (2017).

[5] K. i. Uchida, H. Adachi, T. Kikkawa, A. Kirihara, M. Ishida, S. Yorozu, S. Maekawa, and E. Saitoh, Proceedings of the IEEE **104**, 1946 (2016).

[6] K. Uchida, M. Ishida, T. Kikkawa, A. Kirihara, T. Murakami, and E. Saitoh, Journal of Physics: Condensed Matter **26**, 343202 (2014).

[7] K.-i. Uchida, T. Kikkawa, A. Miura, J. Shiomi, and E. Saitoh, Phys. Rev. X **4**, 041023 (2014).

[8] P. Bougiatioti, C. Klewe, D. Meier, O. Manos, O. Kuschel, J. Wollschläger, L. Bouchenoire, S. D. Brown, J.-M. Schmalhorst, G. Reiss, and T. Kuschel, Phys. Rev. Lett. **119**, 227205 (2017).

[9] R. McLaughlin, D. Sun, C. Zhang, M. Groesbeck, and Z. V. Vardeny, Phys. Rev. B **95**, 180401 (2017).

[10] S. J. Watzman, R. A. Duine, Y. Tserkovnyak, S. R. Boona, H. Jin, A. Prakash, Y. Zheng, and J. P. Heremans, Phys. Rev. B **94**, 144407 (2016).

[11] K.-D. Lee, D.-J. Kim, H. Y. Lee, S.-H. Kim, J.-H. Lee, K.-M. Lee, J.-R. Jeong, K.-S. Lee, H.-S. Song, J.-W. Sohn, S.-C. Shin, and B.-G. Park, Scientific Reports **5** (2015).

[12] S. H. Wang, L. K. Zou, J. W. Cai, B. G. Shen, and J. R. Sun, Phys. Rev. B **88**, 214304 (2013).

[13] A. Slachter, F. L. Bakker, J.-P. Adam, and B. J. van Wees, Nature Physics **6**, 879 (2010).

[14] M. Erekhinsky, F. Casanova, I. K. Schuller, and A. Sharoni, Applied Physics Letters **100**, 212401 (2012).

[15] S. Hu, H. Itoh, and T. Kimura, NPG Asia Materials **6**, e127 (2014).

[16] S. Hu and T. Kimura, Phys. Rev. B **90**, 134412 (2014).

[17] K. Yamasaki, S. Oki, S. Yamada, T. Kanashima, and K. Hamaya, Applied Physics Express **8**, 043003 (2015).

[18] A. Pfeiffer, S. Hu, R. M. Reeve, A. Kronenberg, M. Jourdan, T. Kimura, and M. Klaui, Applied Physics Letters **107**, 082401 (2015).

[19] G.-M. Choi, C.-H. Moon, B.-C. Min, K.-J. Lee, and D. G. Cahill, Nature Physics **11**, 576 (2015).

[20] A. Hojem, D. Wesenberg, and B. L. Zink, Phys. Rev. B **94**, 024426 (2016).

[21] S. Hu, X. Cui, T. Nomura, T. Min, and T. Kimura, Phys. Rev. B **95**, 100403 (2017).

[22] J. Holanda, O. Alves Santos, R. O. Cunha, J. B. S. Mendes, R. L. Rodríguez-Suárez, A. Azevedo, and S. M. Rezende, Phys. Rev. B **95**, 214421 (2017).

[23] S. Y. Huang, W. G. Wang, S. F. Lee, J. Kwo, and C. L. Chien, Phys. Rev. Lett. **107**, 216604 (2011).

[24] A. D. Avery, M. R. Pufall, and B. L. Zink, Physical Review Letters **109**, 196602 (2012).

[25] M. Schmid, S. Srichandan, D. Meier, T. Kuschel, J.-M. Schmalhorst, M. Vogel, G. Reiss, C. Strunk, and C. H. Back, Phys. Rev. Lett. **111**, 187201 (2013).

[26] D. Meier, D. Reinhardt, M. Schmid, C. H. Back, J.-M. Schmalhorst, T. Kuschel, and G. Reiss, Phys. Rev. B **88**, 184425 (2013).

[27] A. von Bieren, F. Brandl, D. Grundler, and J.-P. Ansermet, Applied Physics Letters **102**, 052408 (2013).

[28] S. L. Yin, Q. Mao, Q. Y. Meng, D. Li, and H. W. Zhao, Phys. Rev. B **88**, 064410 (2013).

[29] J.-E. Wegrowe, H.-J. Drouhin, and D. Lacour, Phys. Rev. B **89**, 094409 (2014).

[30] I. V. Soldatov, N. Panarina, C. Hess, L. Schultz, and R. Schäfer, Phys. Rev. B **90**, 104423 (2014).

[31] F. Brandl and D. Grundler, Applied Physics Letters **104**, 172401 (2014).

[32] P. Jayathilaka, D. Belyea, T. Fawcett, and C. W. Miller, Journal of Magnetism and Magnetic

Materials **382**, 376 (2015).

[33] D. Meier, D. Reinhardt, M. van Straaten, C. Klewe, M. Althammer, M. Schreier, S. T. B. Goennenwein, A. Gupta, M. Schmid, C. H. Back, J.-M. Schmalhorst, T. Kuschel, and G. Reiss, Nature Communications **6**, 8211 (2015).

[34] A. S. Shestakov, M. Schmid, D. Meier, T. Kuschel, and C. H. Back, Phys. Rev. B **92**, 224425 (2015).

[35] Y. Cao, C. Feng, D. X. Liu, L. J. Wang, G. Yang, J. Y. Zhang, B. Zhao, S. L. Jiang, Q. Q. Liu, K. Yang, A. B. Zelalem, and G. H. Yu, AIP Advances **6**, 045314 (2016).

[36] O. Reimer, D. Meier, M. Bovender, L. Helmich, J.-O. Dreessen, J. Krieft, A. S. Shestakov, C. H. Back, J.-M. Schmalhorst, A. Htten, G. Reiss, and T. Kuschel, Scientific Reports **7**, 40586 (2017).

[37] J. Sinova, S. O. Valenzuela, J. Wunderlich, C. H. Back, and T. Jungwirth, Rev. Mod. Phys. **87**, 1213 (2015).

[38] A. Hoffmann, Magnetics, IEEE Transactions on **49**, 5172 (2013).

[39] J. E. Hirsch, Phys. Rev. Lett. **83**, 1834 (1999).

[40] M. Dyakonov and V. Perel, Physics Letters A **35**, 459 (1971).

[41] R. Sultan, A. D. Avery, J. M. Underwood, S. J. Mason, D. Bassett, and B. L. Zink, Phys. Rev. B **87**, 214305 (2013).

[42] R. Sultan, A. D. Avery, G. Stiehl, and B. L. Zink, Journal of Applied Physics **105**, 043501 (2009).

[43] V. D. Ky, physica status solidi (b) **22**, 729 (1967).

[44] V. D. Ky, physica status solidi (b) **17**, K207 (1966).

[45] A. D. Avery, M. R. Pufall, and B. L. Zink, Physical Review B **86**, 184408 (2012).

[46] Y. Pu, E. Johnston-Halperin, D. D. Awschalom, and J. Shi, Phys. Rev. Lett. **97**, 036601 (2006).

[47] D. Xiao, Y. Yao, Z. Fang, and Q. Niu, Phys. Rev. Lett. **97**, 026603 (2006).

[48] Y. Pu, D. Chiba, F. Matsukura, H. Ohno, and J. Shi, Phys. Rev. Lett. **101**, 117208 (2008).

[49] T. Böhnert, V. Vega, A.-K. Michel, V. M. Prida, and K. Nielsch, Applied Physics Letters **103**, 092407 (2013).

[50] A. Frauen, A. Kobs, T. Böhnert, A.-K. Michel, G. Winkler, K. Nielsch, and H. P. Oepen, Phys. Rev. B **92**, 140402 (2015).

[51] B. L. Zink, A. D. Avery, R. Sultan, D. Bassett, and M. R. Pufall, Solid State Communications

150, 514 (2010).

[52] A. D. Avery, R. Sultan, D. Bassett, D. Wei, and B. L. Zink, Physical Review B **83**, 100401 (2011).

[53] MATLAB and Partial Differential Equations Toolbox Release 2009a, The MathWorks, Inc., Natick, Massachusetts, United States.

[54] K. Uchida, S. Takahashi, K. Harii, J. Ieda, W. Koshibae, K. Ando, S. Maekawa, and E. Saitoh, Nature **455**, 778 (2008).

[55] K. Uchida, T. Ota, K. Harii, K. Ando, H. Nakayama, and E. Saitoh, Journal of Applied Physics **107**, 09A951 (2010).

[56] A. D. Avery, S. J. Mason, D. Bassett, D. Wesenberg, and B. L. Zink, Phys. Rev. B **92**, 214410 (2015).

[57] S. J. Mason, *Nanoscale Thermoelectrics: A Study of the Absolute Seebeck Coefficient of Thin Films*, Ph.D. thesis, University of Denver (2014).

[58] S. J. Mason, R. K. Bennet, D. Wesenberg, D. Bassett, and B. L. Zink, "Determining absolute Seebeck coefficients from relative thermopower measurements of thin films," (in preparation).